A Poly(propylene imine) (DAB-Am-64) Dendrimer as Cu^{2+} Chelator for the Synthesis of Copper Oxide Clusters Embedded in Sol−Gel Derived Matrixes

Raffet Velarde-Ortiz and Gustavo Larsen*

Department of Chemical Engineering, University of Nebraska, Lincoln, Nebraska 68588-0126

Received August 15, 2001. Revised Manuscript Received October 31, 2001

The fifth generation poly(propylene)imine dendrimer (DAB-Am-64) was used as a macrochelating agent to produce well-dispersed CuO nanoclusters embedded in a silica sol−gel derived matrix. Several characterization methods, including X-ray absorption and diffuse reflectance Fourier transform IR spectroscopies, temperature-programmed oxidation, transmission electron microscopy, and X-ray diffraction, were used for the characterization of the materials. The presence of Cu was found to catalyze the oxidative removal of the dendrimer guest from the silica matrix. The proposed synthetic method, which is expected to be useful for a range of transition metal (e.g., Cu, Ni, Co, Pd, Pt, and Zn) ions with some affinity for amine-type ligands, is viewed as particularly suitable for the synthesis of model supported catalysts and materials with unusual magnetic and optical properties.

Introduction

The technological importance of size control and geometrical arrangement in "quantum dots" is well established.[1,2] In the field of catalysis, particle size control of the active phase is the key to the manipulation of reactivity and selectivity. Physical methods such as formation of reverse miscelles have been used to produce metal and metal oxide aggregates in solution.[3−5] In contrast, chemical methods are even more likely to afford the synthesis of very small metal and metal oxide clusters with extremely narrow particle size windows. The mesoporous SiO_2−Al_2O_3 from Mobil[6,7] and decades of zeolite research[8] are typical examples of nanoengineering design (pore size control as a key goal in this case).

Tomalia et al.[9] and Newkome and co-workers[10] pioneered research in the field of dendrimers, which are highly branched, spheroidal polymers.[11,12] Figure 1 shows a planar projection of the so-called DAB-Am-32 poly(propylene)imine dendrimer. In DAB-Am-32, there are four generations of branches, and the outermost shell is composed of 32 $-NH_2$ groups. The PAMAM (polyamidoamine) family is also a versatile dendrimer class,[13−15] which is able to chelate many Cu(II) ions per molecule.[13,14]

DAB-Am-32

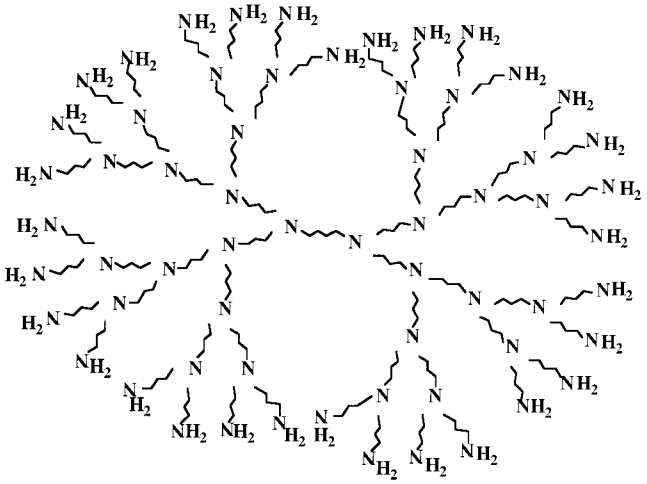

Figure 1. DAB-Am-32: a "generation 4" poly(propylene)imine dendrimer.

* To whom correspondence should be addressed. E-mail: glarsen@unlserve.unl.edu.

(1) Materials Science: Stress-free carbon needs no support. Special steel finds real applications. Quantum dots into a 3-D array. *Sci. News* (*Washington, D. C.*) **1998**, *154*, 383.
(2) MIT team uses simple path to make highly ordered 3-D arrays (superlattices) of semiconductor nanocrystals that offer potential uses. *Chem. Eng. News* **1995**, *73*, No. 48, 6.
(3) Pileni, M. P. *New J. Chem.* **1998**, *22*, 693.
(4) Lin, X. M.; Sorensen, C. M.; Klabunde, K. J.; Hadjipanayin, G. C. *Langmuir* **1998**, *14*, 7140.
(5) Lopez Perez, J. A.; Lopez Quintela, M. A.; Miras, J.; Rivas, J.; Charles, S. W. *J. Phys. Chem. B* **1997**, *101*, 8045.
(6) Beck, J. S.; Vartuli, J. C.; Roth, W. J.; Leonowicz, M. E.; Kresge, C. T.; Schnitt, K. D.; Chu, C. T−W.; Olson, D. H.; Sheppard, E. W.; McCullen, S. B.; Higgins, J. B.; Schlenker, J. L. *J. Am. Chem. Soc.* **1992**, *114*, 10834.
(7) Kresge, C. T.; Leonowicz, M. E.; Roth, W. J.; Vartuli, J. C.; Beck, J. S. *Nature* **1992**, *359*, 710.
(8) Davis, M. E. *Acc. Chem. Res.* **1993**, *23*, 111.
(9) Tomalia, D. A.; Baker, H.; Dewald, J. R.; Hall, M.; Kallos, G.; Martin, S.; Roeck, J.; Ryder, J.; Smith, P. *Macromolecules* **1986**, *19*, 2466.
(10) Newkome, G. R.; Yao, Z.-Q.; Baker, G. R.; Gupta, K. *J. Org. Chem.* **1985**, *50*, 2003.
(11) Tomalia, D. A.; Naylor, A. M.; Goddard, W. A., III *Angew. Chem.* **1990**, *29*, 138.
(12) Bosman, A. W.; Janssen, H. M.; Meijer, E. W. *Chem. Rev.* **1999**, *99*, 1665.
(13) Balogh, L.; Tomalia, D. A. *J. Am. Chem. Soc.* **1998**, *120*, 7355.
(14) Zhao, M.; Sun, L.; Crooks, R. M. *J. Am. Chem. Soc.* **1998**, *120*, 4877.
(15) Chechik, V.; Zhao, M.; Crooks, R. M. *J. Am. Chem. Soc.* **1999**, *121*, 4910.

10.1021/cm010754s CCC: $22.00
Published on Web 01/12/2002

The advantage of using dendrimers to make dendrimer−inorganic hybrids is 2-fold: First, DAB-Am-*n* and PAMAMs can be used as monomolecular pore templates to produce silicas with quasi-spherical cavities, upon calcination of the composite.[16−18] Second, the chelating capacity of such amine dendrimers can be used to trap metal ions in the composites to ultimately make, after high-temperature and oxidation/reduction treatments, embedded metal oxide and metal clusters of tunable sizes.

The main focus of this contribution is to report on the dendrimer-mediated synthesis and characterization of CuO nanoclusters embedded in a silica sol−gel matrix. Nanosized CuO clusters supported on inert oxide carriers catalyze the reduction of nitrogen oxide gases in the presence of hydrocarbons[19] and are often found to be ferromagnetic when embedded in silica matrixes.[20] The strategy of dendrimer-mediated embedding of small metal and metal oxide particles that is proposed in this paper, which is not limited to just copper, is viewed as complementary to that of surface grafting and adsorption proposed by other authors.[21,22] Our strategy will be particularly suited for catalysis with small molecules (that can diffuse rather easily through a porous glass) and other applications requiring entrapment of the particles to prevent undesirable phenomena such as high-temperature sintering.

In a recent publication, we "stained" the sol−gel trapped DAB-Am-*n* dendrimers with Cu^{2+} ions to improve contrast for transmission electron microscopy imaging purposes.[16] Almost at the same time, Ruckenstein and Yin[23] reported on a similar strategy to incorporate copper in silica/PAMAM dendrimer composites. Very recently, PAMAMs were copolymerized with 2-hydroxyethyl methacrylate, and the resulting polymer was swollen with $AgCl_4^-$ and $PtCl_6^{2-}$ solutions to effect, upon chemical treatment, the formation of trapped transition metal nanoclusters.[24] In solution, the use of dendrimers to make model metal clusters is clearly in a more advanced state.[25,26] Some of the work presented in this manuscript is related to that of dendrimer-mediated synthesis of 2-D Zn arsenates.[27]

Experimental Section

Preparation of Materials. All reagents were from Aldrich and used as received. A series of samples were prepared with variable Cu^{2+}/DAB-Am-64 molar ratios. Since the properties of these materials were found to vary monotonically with Cu content, this study primarily focuses on one composition, namely, that with a Cu^{2+}/DAB-Am-64 ratio of 16. The maximum Cu^{2+}/DAB-Am-64 molar ratio in solution, according to Vassilev and Ford,[28a] is 32. While these authors' argument is not definitive, a Cu^{2+}/DAB-Am-64 ratio of 16 is expected to be well below the total chelating power of the dendrimer. Complexation of Cu^{2+} by poly(propylene imine) dendrimers was first reported by Bosman et al.[28b]

The material, labeled as CuD16, was prepared as follows: 250 mg of DAB-Am-64 was dissolved in 1.3 mL of 2-propanol followed by addition of 0.5 mL of a 0.03 M methanolic solution of $Cu(NO_3)_2 \cdot 2.5H_2O$ and 3.0 mL of deionized water. This gave the classical deep blue coloration associated with Cu^{2+} amine complexes. To this mixture, 1.0 mL of a 3.08 M methanolic solution of tetraethylortosilicate (TEOS) was added. The mixture was placed in a closed container at 348 K for 3 h and then for another 12 h at the same temperature in an open container. The resulting solid was oven dried at 373 K for 12 h after which it turned green and was finally ground to fine powders.

Characterization. *Temperature-Programmed Oxidation (TPO) Experiments.* To study the thermal decomposition patterns of our materials, a computer-interfaced MKS mass spectrometer (MS) was used. The experimental setup, which consists of a flow-through cell and associated mass-flow and temperature controllers, is described in detail elsewhere.[29] In brief, samples were redried at 383 K for 30 min prior to TPO runs. Typically, 0.08 g of the sample was placed in the TPO cell as a 1:2 sample/SiO_2 (Fluka, nonporous) mixture along with a preheating bed of nonporous α-Al_2O_3. A 1:1 He/UHP air feed flow (40 cm^3/min) was set. The gas phase was sampled for MS analysis as described earlier.[29] The final temperature (1100 K) was achieved by means of a 3.33 K/min ramp. Up to 16 different masses were carefully selected to follow potential total and partial oxidation products and alkenes,[29] but only very few *m*/*e* ratios gave significant signals.

Diffuse Reflectance IR Fourier Transform Spectroscopy (DRIFTS). All spectra were collected on a computer-interfaced Nicolet 20SXB Fourier transform IR spectrometer equipped with a commercial DRIFTS cel, and associated optical and temperature control systems from Spectratech. Typically, the sample (ca. 0.05 g) was placed in the DRIFTS cell and redried under flowing UHP air at 383 K for 30 min, and spectra were then collected in the wavenumber interval of 4000−400 cm^{-1} (500 scans at a resolution of 4 cm^{-1}).

Surface Area Analysis. BET specific surface areas were derived from nitrogen physisorption data at 77 K, using a custom-built greaseless glass line equipped with a Baratron pressure transducer, mechanical and diffusion pumps, and bakeable three O-ring Teflon stopcocks. Prior to the measurements, the sample was evacuated for 1 h at 383 K.

Powder X-ray Diffraction. A Cu Kα-based Rigaku DBMax II instrument was used.

Transmission Electron Microscopy (TEM). TEM studies were conducted in the bright-field mode with a JEOL JEM2010 microscope at 200 keV beam energy. The powders were deposited on conventional carbon-coated Cu grids.

XAS Data Collection. Cu K edge XAS data were acquired in the transmission mode at room temperature on the X18B beamline at the National Synchrotron Light Source. Spectra were obtained by using three N_2-filled gas ionization chambers as detectors, with the sample placed between the first and second chambers and a Cu foil between the second and third chambers as an internal standard. Special care was taken to prepare pellets with adequate optical thickness. The energy resolution of the beam was 1.5 eV.

(16) Larsen, G.; Lotero, E.; Marquez, M. *Chem. Mater.* **2000**, *12*, 1513.
(17) Larsen, G.; Lotero, E.; Marquez, M. *J. Mater. Res.* **2000**, *15*, 1842.
(18) Larsen, G.; Lotero, E.; Marquez, M. *J. Phys. Chem. B* **2000**, *104*, 4840.
(19) Chajar, Z.; Le Chanu, V.; Primet, M.; Praliaud, H. *Catal. Lett.* **1998**, *52*, 97.
(20) Garcia, N.; Crespo, P.; Hernando, A.; Bovier, C.; Serughetti, J.; Duval, E. *Phys. Rev. B* **1993**, *47*, 570.
(21) Bourque, S. C.; Alper, H.; Manzer, L. E.; Arya, P. *J. Am. Chem. Soc.* **2000**, *122*, 956.
(22) van Duijvenbode, R. C.; Koper, G. J. M.; Böhmer, M. R. *Langmuir* **2000**, *16*, 7713.
(23) Ruckenstein, E.; Yin, W. *J. Polym. Sci., Part A: Polym. Chem.* **2000**, *38*, 1443.
(24) Gröhn, F.; Kim, G.; Bauer, B. J.; Amis, E. J. *Macromolecules* **2001**, *34*, 2179.
(25) Crooks, R. M.; Lemon, B. I., III; Yeung, L. K.; Zhao, M. *Top. Curr. Chem.* **2000** *212*, 81.
(26) Balogh, L.; Laverdure, K. S.; Gido, S. P.; Mott, A. G.; Miller, M. J.; Ketchel, B. P.; Tomalia, D. A. *Mater. Res. Soc. Symp. Proc.* **1999**, *576*, 69.
(27) Lotero, E.; Spretz, R.; Larsen, G. *Chem. Mater.*, in press.
(28) (a) Vassilev, K.; Ford, W. T. *J. Polym. Sci.* **1999**, *37*, 2727. (b) Bosman, A. W.; Schenning, A. P. H. J.; Janssen, R. A. J.; Meijer, E. W. *Chem. Ber.* **1997**, *130*, 725.
(29) Lotero, E.; Vu, D.; Nguyen, C.; Wagner, J.; Larsen, G. *Chem. Mater.* **1998**, *10*, 3756.

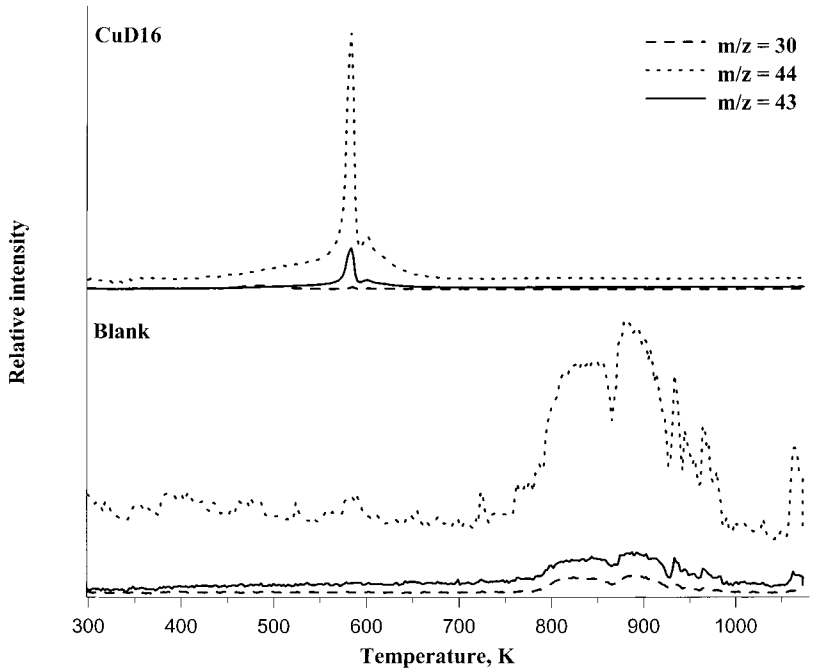

Figure 2. TPO patterns of CuD16 (upper panel) and blank sample.

Extended X-ray Absorption Fine Structure (EXAFS) Analysis. Data reduction was done by using the WinXAS program suite,[30] which has an interface to generate theoretical phase and amplitude functions from the FEFF 8.10 program (Rehr and co-workers).[31] Input files for FEFF 8.10 were generated by using the WebATOMS[32] database or by building molecular models of simple geometries whose Cartesian coordinates were exported into a FEFF input file. In all fitting procedures, the amplitude reduction factor (So^2) was set to one and only SS paths were considered. Fitting of the EXAFS data was done in *k* space.

X-ray Absorption Near-Edge Structure (*XANES) Analysis*. Theoretical simulations of XANES spectra were also obtained with the aid of the FEFF 8.10 software. A large number of hypothetical structures were generated based on regular tetrahedral, square planar, square pyramidal, and octahedral geometries with the first coordination shell containing nitrogens in the form of imidazol rings and at least one oxygen ligand. The purpose of the XANES analysis was to gain some insight into the structure of uncalcined CuD16. Oxygen needs to be considered as a potential nearest neighbor because the trapped, Cu-loaded dendrimer is obviously embedded in an O-rich environment and has charge-balancing NO_3^-. In models where better matching to the experimental XANES was observed, several other Cu−O and Cu−N distances were tried. The Cartesian coordinates of all atoms in the model were exported into a FEFF input file.

Results and Discussion

Basic Textural Properties. Prior to the study of the finer details of the structure of this material before and after calcination by means of spectroscopy, basic textural features needed to be evaluated. The TPO experiments, for example, were primarily aimed at determining the impact of Cu on the calcination process. The TPO decomposition patterns of CuD16 and that of a blank material, prepared by simply omitting the presence of Cu^{2+} in the methanol/water solution in the synthetic scheme described above, are shown in Figure 2. The figure shows *m/e* values of 44 (CO_2^+ fragment), 30 (NO^+; from nitrogen oxides), and 43 (alkanes; to check for pyrolytic, non-oxidative pathways). In our previous work,[16,17] we used calcination temperatures in the 800−850 K range for 1−3 h to completely eliminate the dendrimer in DAB-Am-*n*/silica (transition metal free) materials. The blank TPO curve in this study is consistent with our previous work. As anticipated, much lower temperatures were required for complete removal of carbonaceous matter when Cu was present, since most transition metals have a catalytic effect for temperature-programmed oxidative eliminations in sol−gel glasses.[29,33] Note that the TPO data in Figure 2 confirms that no additional CO_2 evolves past the 700 K mark. The calcination temperature of CuD16 prior to XAS and TEM data collection was selected according to TPO data, since we wanted to effect complete carbon removal but at the same time minimize thermal changes that might occur at elevated temperatures (loss of surface area, aggregation, etc.).

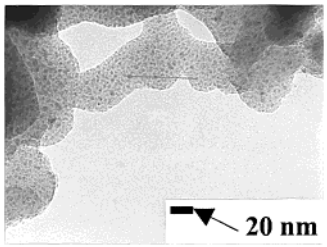

Figure 3. TEM image of calcined CuD16.

The BET specific surface areas of the blank and CuD16 samples were found to be 416.9 and 290.5 m^2/g, respectively. A TEM image of calcined CuD16 is shown in Figure 3. While there are obvious signs of high Cu

(30) Ressler, T. Ph.D. Thesis, University of Hamburg, Germany, 1995.

(31) Ankudinov, A. L.; Ravel, B.; Reher, J. J.; Conradson, S. D. *Phys. Rev.* **2000**, *B62*, 7665.

(32) This Archive is a collection of crystallographic data for use in XAFS analysis: http://cars9.uchicago.edu/~newville/adb/.

(33) Larsen, G.; Buechler-Skoda, M.; Nguyen, C.; Vu, D.; Lotero, E. *J. Non-Cryst. Solids* **2001** *279*, 161.

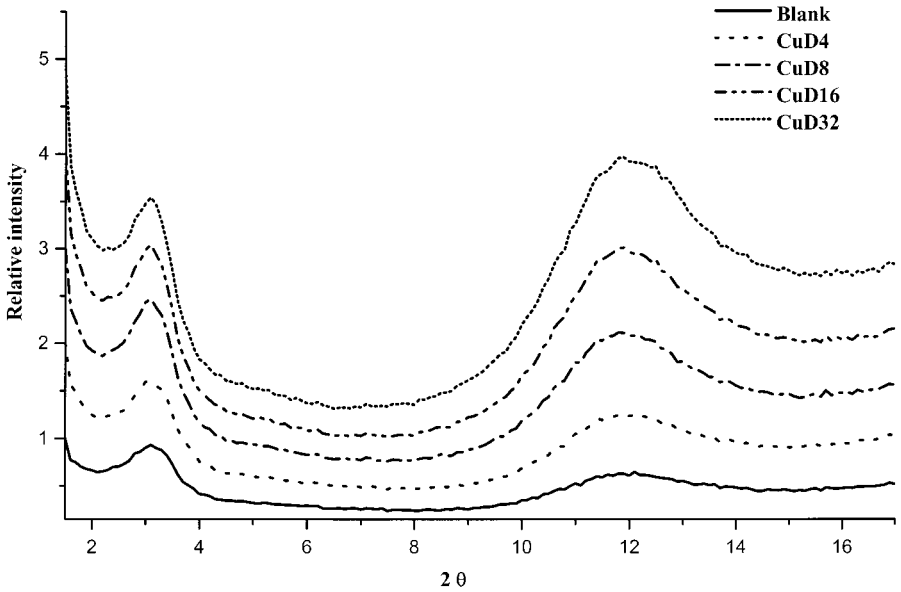

Figure 4. Low-angle X-ray diffraction patterns of CuD series (dried at 383 K) and blank.

dispersion and the size distribution of the CuO particles appears to be rather narrow, no clear indication of supralattice formation (2- or 3-D ordering of the embedded CuO particles) was found. The TEM image in Figure 3, in terms of both high dispersion and lack of 2- or 3-D ordering, is qualitatively similar to those of the uncalcined materials reported earlier.[16]

The XRD patterns of an oven-dried CuD series (where the suffix represents the Cu^{2+}/DAB-Am-64 ratio) are shown in Figure 4. The low-angle XRD data confirms our hypothesis about the low level of ordering in these materials, as only one peak below $2\theta = 10°$ is observed at ca. 3.2°. The latter corresponds closely to the DAB-Am-64 diameter.[16,17] The reflection at $2\theta = 12°$ (Bragg distance of ca. 7.5 Å) is much more intriguing. It increases monotonically in intensity as the Cu content increases. In these materials, Cu is the highest-Z element and as such it is the strongest X-ray scatterer. The filling of the dendrimer volume with Cu^{2+} ions appears to reveal scattering centers that are approximately 7.5 Å apart. Given the expected charge separation requirements upon gelation, it is reasonable to assume that these rather disordered CuO nanocluster/silica composites are also forced to keep at least one extra XRD-coherent length in addition to that related to dendrimer size. Once these Cu-containing materials are calcined (and unlike their Cu-free analogues[16,17]), the low 2θ signal decreases significantly in intensity whereas the signal at 12° remains essentially unchanged. No XRD evidence was found for the presence of Cu phases after calcination (e.g., CuO, Cu_2CO_3, etc.). This does not preclude formation of CuO clusters, as very small particles are expected to be "XRD amorphous".

DRIFTS and XAS. As the electron demand on the nitrogen atoms increases by Cu^{2+} complexation, the polarity and thus the permanent dipole moment (and IR intensities) of the N−H bonds increase.[34] The progression of the N−H region (3050−3500 cm^{-1}) as a function of Cu content in the DRIFTS spectrum of the oven-dried CuD*n* materials is in agreement with this principle (Figure 5). Furthermore, it indicates that trapped Cu^{2+}−DAB-Am-64 complexes involve participation of the terminal (primary) amine groups, as recently suggested in solution.[28] The antisymmetric (3380 cm^{-1}) and symmetric (3300 cm^{-1}) N−H stretching modes appear as a well-defined doublet in the Cu-free material and in the sample with the lowest Cu concentration. However, a complex band splitting sets in as the Cu content is increased, suggesting the existence of multiple Cu^{2+}−NH_2 coordinations.

The antisymmetric and symmetric CH_2 stretching signals (2950 and 2850 cm^{-1}, respectively) are somewhat masked by the dramatic increase in intensity of the N−H IR bands. Any impact of Cu^{2+} complexation on the C−H region would not be detectable because this would be a second-order effect. However, a band at 2900 cm^{-1} becomes evident as the Cu content increases. In alkylammonium salts, protonation gives rise to an IR band at ca. 2900 cm^{-1},[35] which is normally attributed to symmetric $-NH_3^+$ stretching. If complexation of terminal $-NH_2$ groups by Cu^{2+} ions has an effect on the N−H bond that is qualitatively similar to that of protonation, the 2900 cm^{-1} signal could in principle be ascribed to this phenomenon. The main idea derived from DRIFTS analysis is that there is heavy involvement of the "shell" (terminal) N atoms of the dendrimer in the anchoring of Cu^{2+} ions to the dendrimer/sol−gel composite.

Prior to XAS analysis, it must be mentioned that electron paramagnetic resonance (EPR) proved of little use with these materials. There was a tendency in these oven-dried (383 K) solids to produce a very broad EPR signal that is characteristic of Cu^{2+} ions that are close enough to one another to effectively smear out any hyperfine structure via dipolar coupling.[36] Thus, EPR offered qualitative indication that the Cu-containing

(34) Svatos, G. F.; Curran, C.; Quagliano, J. V. *J. Am. Chem. Soc.* **1955**, *77*, 6159.

(35) Several IR group frequency tables are available online. See, for example, http://www.lure.u-psud.fr/Experiences/SACO/SA5/Communs/tab_freq.htm.

(36) Centi, G.; Perathoner, S.; Biglino, D.; Giamello, D. *J. Catal.* **1995**, *151*, 75.

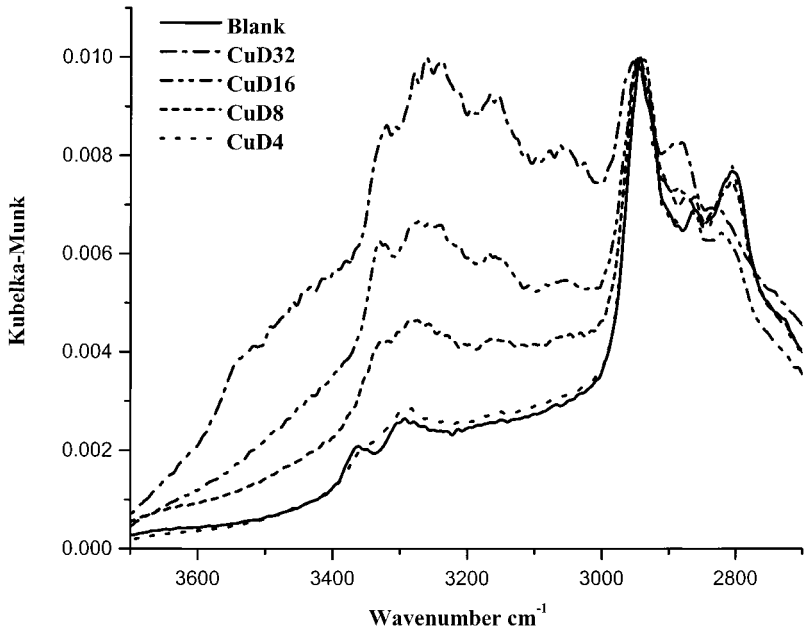

Figure 5. DRIFTS spectra of CuD materials dried at 383 K.

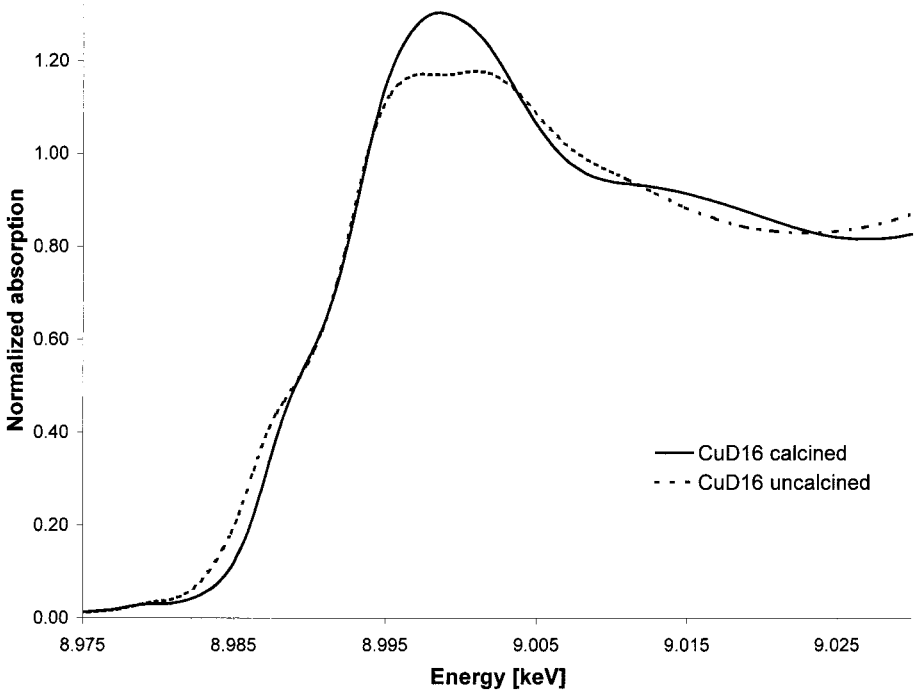

Figure 6. XANES spectra of calcined and uncalcined CuD16.

trapped dendrimers appear to favor $Cu^{2+}-Cu^{2+}$ interactions. These EPR observations do not necessarily suggest that the spatial distribution of spin-interacting Cu^{2+} centers within the dendrimer cannot be random, as discussed later in light of XAS data.

The XANES of uncalcined CuD16 exhibit features characteristic of Cu(II) complexes[37] (Figure 6). To gain better insight into the local structure around Cu^{2+} ions, a series of theoretical XANES were generated and compared against the experimental XANES. Peaks at 8.977 keV (symmetry forbidden 1s → 3d transition[36]) and 8.987 keV (1s → 4pπ transition)[37] and the twin peaks at 8.996 and 9.001 keV (1s → 4pσ transition)[37] were hard to reproduce for most local geometries. Upon considerable effort, some qualitative features of the experimental XANES were reproduced with a square pyramidal model, where the first coordination shell is formed by three equatorial N atoms (Cu−N 1.99 Å) and one equatorial and one axial O atom (Cu−O 2.5 Å). It is obvious that this square pyramidal model, the closest match we could find, also departs from the experimental XANES (Figure 7). However, we should also mention that model clusters with either N or O single first shells deviated even more from the experimental XANES of uncalcined CuD16 (for example, a lack of the 8.997−9.001 keV doublet), which indicated that both N and O

(37) Kau, L.-S.; Spira-Solomon, J.; Penner-Hahn, J. E.; Hodgson, K. O.; Solomon, E. I. *J. Am. Chem. Soc.* **1987**, *109*, 6433.

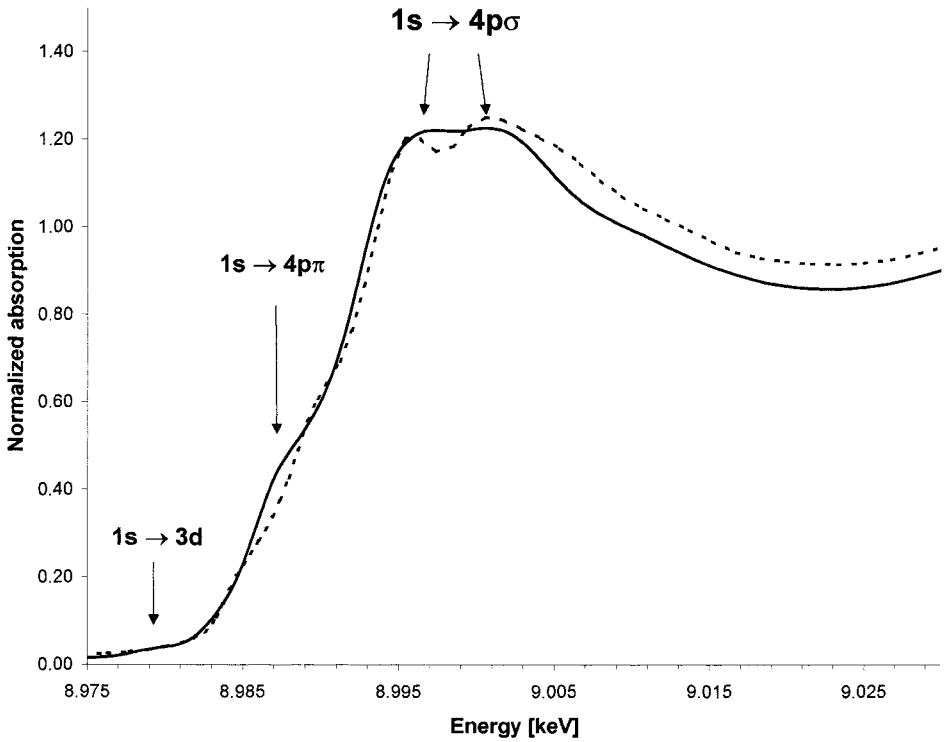

Figure 7. XANES spectrum of uncalcined CuD16 (solid) and simulated XANES profile.

interact with Cu^{2+}, and both are needed for EXAFS analysis.

The twin peaks energy position (8.996 and 9.001 keV) in the theoretical XANES is in good agreement with that observed in uncalcined CuD16, but the intensity of the peaks was overestimated. One possible explanation for the broadening of the twin peaks lies in the flexibility of the dendrimer structure trapped in the sol−gel (see the broad XRD reflections in Figure 4). Heterogeneity in the electronic environment around the Cu^{2+} ions is expected if the dendrimer branches are allowed to have conformational flexibility. A similar proposal was made in previous XANES studies of enzyme−Cu^{2+} systems, where site heterogeneity led to a poorly defined doublet relative to that predicted by theory.[40] In summary, the XANES analysis provides qualitative clues as to how to model the Cu^{2+} EXAFS of uncalcined (N and O mixed first shell) and calcined (single O-shell) CuD16. Given that XANES theoretical models that were based solely on N ligands (with and without equivalent distances) were unable to reproduce the twin peak feature, use of a mixed (N/O) first shell to model the EXAFS of uncalcined CuD16 was viewed as essential. The DRIFTS data suggest heavy involvement of the primary amine groups of DAB-Am-64 in coordinating Cu^{2+}, and the low resolution of both the XRD signals and the Cu XANES twin peaks at 8.997 and 9.001 keV point to the flexibility of the dendrimer structure to exist in a distribution of conformations once trapped in this silica sol−gel matrix.

To derive structural parameters from EXAFS in uncalcined CuD16, ab initio phase shift and amplitude functions were generated by using an approximate square planar model where two copper atoms are bound to two imidazole groups each, and in turn, these single Cu^{2+} centers are bridged by one nitrogen and one oxygen atom. This cluster model serves two purposes: First, either half of the cluster can be used to fit the N/O first coordination sphere. Second, each half represents the equatorial environment of the square pyramidal model used for XANES, as described earlier. Another purpose of the theoretical reference structure adopted was to attempt to model the clustering of the Cu^{2+} centers, as suggested by EPR, in case such Cu^{2+}−Cu^{2+} interactions were not random and thus EXAFS-silent.

Figure 8 shows the isolated EXAFS function of uncalcined CuD16 and its Fourier transform magnitude. The mathematical stability of mixed-shell EXAFS fitting, especially with shell elements having very similar atomic numbers, has long been questioned for being a classical case of a problem with a large number of free parameters. Therefore, we decided to test two different approaches to model the uncalcined CuD16 first shell. One only considered the Cu−N contribution and the other took into account both the Cu−N and Cu−O parts of the theoretical reference cluster. Results are shown in Table 1. Figures 1a and 1b in the Supporting Information illustrate the inability of a single N shell to accurately model the EXAFS data of uncalcined CuD16. It is clear that the inclusion of the Cu−O shell greatly improves the quality of the fit. In our case, the counterion was NO_3^- ($Cu(NO_3)_2$ was used as a Cu^{2+} precursor), which is expected to be in close proximity to the Cu^{2+} cations prior to calcination of the materials. It is noteworthy that a Cu−N coordination number of about 2 is consistent with known chemistry of Cu^{2+}/DAB-Am-*n* in water,[28] whereas 4-fold oxygen coordination could be the result of either charge neutralization (two bidentate NO_3^- ions interacting with Cu^{2+}) or a

(38) Shulman, R. G.; Yafet, T.; Eisenberger, P.; Blumberg, W. E. *Proc. Natl. Acad. Sci.* U.S.A. **1976**, *73*, 1348.
(39) Kosugi, N.; Kondoh, H.; Tajima, H.; Kuroda, H. *Chem. Phys.* **1989**, *135*, 149.
(40) Scott, R. A.; Dooley, D. M. *J. Am. Chem. Soc.* **1985**, *107*, 4348.

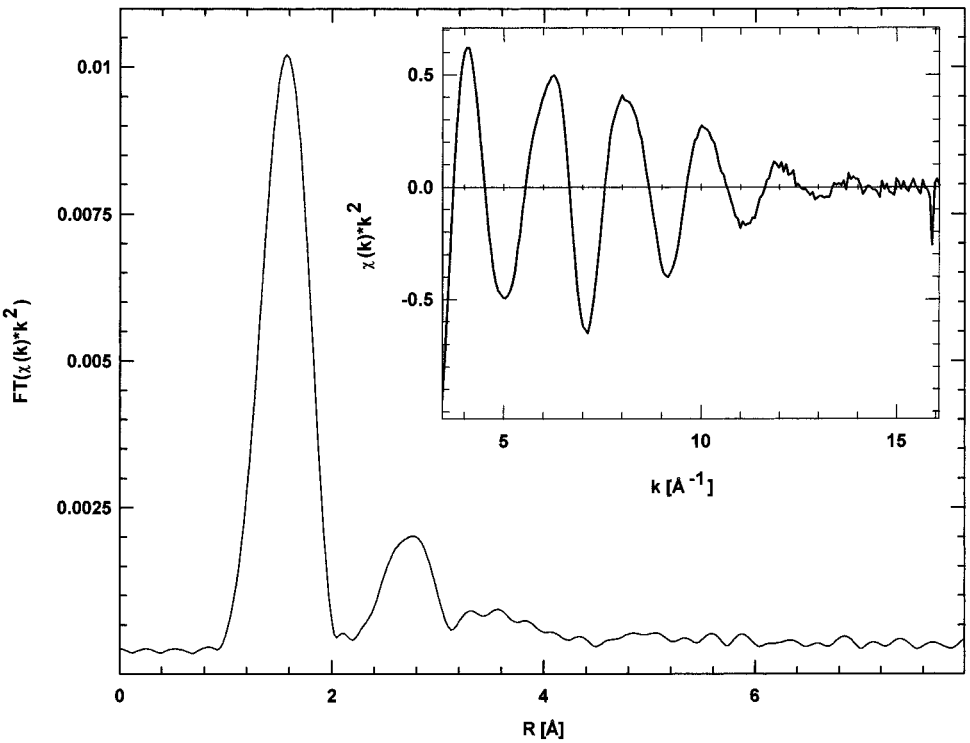

Figure 8. The k^2-weighted EXAFS of uncalcined CuD16 (inset) and its FFT magnitude.

Table 1. First-Shell EXAFS Modeling Results for Uncalcined CuD16[a]

parameter	single shell **1**	mixed shell **1**, **2**
coord no., *N*	1.97	2.2, 4.5
distance, *R* (Å)	2.02	1.92, 2.22
$\Delta\sigma^2$ (Å^2)	0.0016	0.0040, 0.0090
rel res error	50.2	16.225

[a] Reference: **1**: (Cu−N) $N = 3.0$, $R = 1.99$ Å; **2**: (Cu−O) $N = 1.0$, $R = 2.5$ Å.

Table 2. Second-Shell EXAFS Modeling Results for Uncalcined CuD16[a]

parameter	single shell **1**	single shell **2**	mixed shell **1**, **2**
coord no., *N*	3.6	18.2	3.2, 0.1
distance, *R* (Å)	3.06	2.93	3.03, 3.10
$\Delta\sigma^2$ (Å^2)	0.0085	0.0524	0.0079, 0.0026
rel res error	22.676	54.128	17.508

[a] Reference: **1**: (Cu−C) $N = 2.0$, $R = 2.96$ Å; **2**: (Cu−Cu) $N = 1.0$, $R = 3.08$ Å.

combination of charge neutralization and interaction of Cu^{2+} with O from the sol−gel matrix.

EXAFS analysis beyond the first coordination sphere to determine metal−metal distances is normally a rather difficult task.[41,42] To model the second shell of uncalcined CuD16, three approaches were tested. One considered a Cu−Cu and Cu−C mixed shell, and the two remaining ones corresponded to pure Cu−Cu and Cu−C contributions. Rather than the univocal determination of whether C, O, or N (or any combination of all three) are the primary contributors to the EXAFS second shell, the goal of second-shell analysis was to investigate the potential occurrence of a preferential and EXAFS detectable Cu−Cu distance, which could be easily distinguishable (given the strong backscattering properties of Cu at high *k*) from any of the low-Z element (C, O, or N) contributions. Results are summarized in Table 2. The model based on Cu only resulted in a poor fit (note the large residual error) with an unrealistic coordination number. Those based on a Cu−C/Cu−Cu mixed shell and a single Cu−C shell are of good quality, and clearly show that the Cu−Cu distances in these materials are not EXAFS-coherent to any significant extent. Parts a−c of Figure 2 (Supporting Information) show the fitting of the isolated second-shell EXAFS function of uncalcined CuD16 to each type of single and double reference second shell adopted here. Our EXAFS results imply that Cu^{2+} centers, which interact with each other electronically (EPR), *are not geometrically arranged* within the dendrimers.

A hypothetical $Cu_6O_{16}^{20-}$ cluster with tenorite (natural CuO) structure is shown in Figure 9 (lower panel). The primary building unit in tenorite is the Jahn−Teller distorted planar CuO_4 center (Figure 9, upper picture), which in turn is responsible for the occurrence of two Cu−O distances in the Cu first shell.[44] The two O atoms at ca. 2.78 Å are too far to be considered as part of the Cu first shell. The first-shell Cu−O distortions translate into multiple Cu−Cu second-shell distances (Figure 9, middle). The three structures in Figure 9 were constructed with the web version of Bruce Ravel's ATOMS program[45] and will be illustrative when discussing the results of EXAFS analysis of calcined CuD16.

(41) Riggs-Gelasco, P. J.; Stemmler, T. L.; Penner-Hanh, J. E. *Coord. Chem. Rev.* **1995**, *144*, 245.
(42) Scott, R. A.; Eidsness, M. K. *Comments Inorg. Chem.* **1988**, *7*, 235.
(43) DuBois, J. L.; Muhkerjee, P.; Collier, A. M.; Mayer, J. M.; Solomon, E. I.; Hedman, B.; Stack, T. D. P.; Hodgson, K. O. *J. Am. Chem. Soc.* **1997**, *119*, 8578.
(44) Asbrink, S.; Norby, L.-J. *Acta Crystallogr., Sect. B* **1970**, *26*, 8.
(45) Ravel, B. The ATOMS program to calculate radial distances is also available online at: http://cars9.uchicago.edu/cgi-bin/atoms/atoms.cgi?file=CuO.inp.

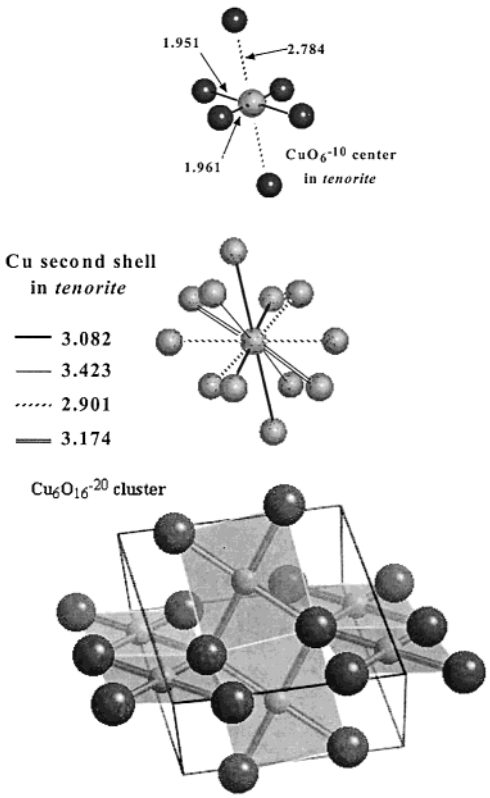

Figure 9. Basic building blocks of the CuO structure.

Table 3. First-Shell EXAFS Modeling Results for Calcined CuD16[a]

parameter	single shell **1**	single shell **2**	mixed shell **1**, **2**	mixed shell **1**, **2**[b]
coord no., N	1.9	1.9	2.4, 0.1	2.5, 0.6
distance, R (Å)	1.97	1.97	1.98, 1.84	1.98, 1.85
$\Delta\sigma^2$ (Å^2)	0.0004	0.0004	0.0012, −0.0015	0.0019, 1×10^{-6}
rel res error	46.9	46.9	13.1	13.9

[a] Reference: **1**: $N = 2.0$, $R = 1.9509$ Å; **2**: $N = 2.0$, $R = 1.9610$ Å. [b] Placing a $\Delta\sigma^2 > 0$ constraint.

In our materials, the silica-encaged CuO clusters were a priori expected to experience saturation of the Cu first shell with O^{2-} ions, which is not uncommon in encaged nanoclusters. Vaarkamp et al.[44] modeled Pt clusters inside L-zeolite channels by EXAFS and concluded that the zeolite cages were responsible for Pt−O distances in Pt^0 clusters.

Figure 10 shows the isolated k^2-weighted EXAFS function of the calcined CuD16 material and its Fourier transform magnitude. Figure 3 in the Supporting Information shows the isolated first-shell EXAFS function and the corresponding k-fit. The first-shell EXAFS data analysis for calcined CuD16 is summarized in Table 3.

Since Cu^{2+} in CuO has two O^{2-} ions at $R_1 = 1.9509$ Å and the remaining two at $R_2 = 1.9610$ Å, the possibility of doing both single- and mixed-shell analysis of the filtered EXAFS Cu−O function needed to be evaluated carefully. Such Jahn−Teller distortion automatically calls for a mixed-shell model while remaining on guard against potential mathematical instabilities in the fitting process, as mentioned earlier. Thus, Table 3 shows EXAFS modeling results using the two Cu−O distances in tenorite independently (one shell) as starting points and in combination. Given the small difference between the two types of Cu−O bonds, both single-shell models naturally fall into the same minimum.

Table 4. First-Shell EXAFS Results for Calcined CuD16; A Single Cu−Cu Second-Subshell Reference from Tenorite (Natural CuO, $R = 2.9007$ Å, $N = 4.0$) Was Used as Reference

parameter	k-space	parameter	k-space
coord no., N	3.7	$\Delta\sigma^2$ (Å^2)	0.0015
distance, R (Å)	2.97	rel res error	26.00

Assumption of a ±15% error in the value of N when modeling EXAFS data of good quality is customary (note the low signal/noise ratio at very high k in Figure 10). The two single-shell fits in k-space resulted in rather large errors but nevertheless low coordination numbers. If one assumes that a mixed-shell model is more appropriate in distorted Cu^{2+} centers, the latter still predicts unsaturation of the Cu first O-shell in calcined CuD16. In general, our effort to fit the data adequately with a single first shell failed. By simple inspection, there were obvious qualitative differences between the standard EXAFS function and that of the sample. It is particularly noteworthy that a measurable contribution of a short Cu−O distance to the Cu EXAFS was always present. The two mixed-shell data columns present the fitting of XAS data under no constraints and under the forcing of the $\Delta\sigma^2$ parameters to be larger than zero. Nevertheless, no significant differences were observed in the quality of the fits and in the output parameters.

In superconducting cuprates,[47] the so-called CuO_2 sheets are locally similar to the square planar $(CuO_2)_n$ ribbons depicted in Figure 9 (lower panel). However, hole-doping (e.g., La^{3+}) shortens the Cu−O bond distance markedly.[47] Our EXAFS analysis indicates that the silica-embedded CuO nanoclusters must possess a relatively high population of defects or holes to account for the presence of a Cu−O distance of 1.82−1.85 Å, which is the most desirable property for catalysis and adsorption applications. An alternative explanation for the short Cu−O distance observed in CuD16 would be the presence of Cu^+ or better a Cu_2O phase. Despite its lower oxidation state, Cu_2O has a Cu−O bond length of 1.84 Å.[48] However, this possibility can be ruled out on the basis of the fact that no evidence for the well-known 8.984 keV 1s → 4s transition of Cu(I) was found in the XANES of calcined CuD16 (Figure 6).[37] Instead, the weak shoulder at 8.987 keV associated with ionic Cu^{2+} materials was seen.[36,37] The K edge of the rather unusual Cu^{3+} also shows a pronounced pre-edge feature below 8.984 keV,[39] but such signal was absent in calcined CuD16. Thus, we favor the hole formation hypothesis, as in M^{3+}-subsituted cuprates, to account for the short C−O distance, and the presence of tetravalent Si could in principle be a cause for it.

To gain better insight into the size of the CuO nanoclusters, second-shell EXAFS analysis was carried out (see Table 4 and Figure 4 in Supporting Information). For the Cu−Cu shell case, a single-shell model was sufficient to produce satisfactory results. Obviously, a minimum of four Cu−Cu distances exist even in the bulk (Figure 9, middle), possibly with some overlapping Cu−O (second shell) contribution. However, our goal

(46) Vaarkamp, M.; Modica, F. S.; Miller, J. T.; Koningsberger, D. C. *J. Catal.* **1993**, *144*, 611.
(47) Rao, C. N. R.; Ganguli, A. K. *Chem. Soc. Rev.* **1995**, *24*, 1.
(48) Sankar, G.; Thomas, J. M.; Waller, D.; Couves, J. W.; Catlow, C. A. R.; Greaves, G. N. *J. Phys. Chem.* **1992**, *96*, 7485.

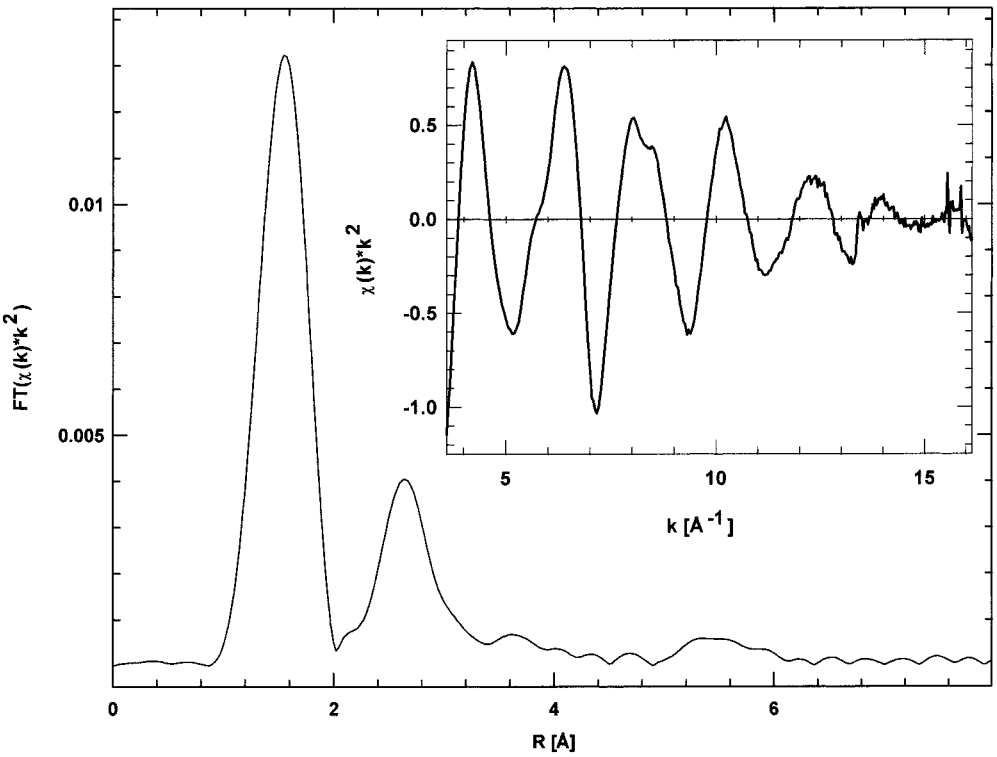

Figure 10. The k^2-weighted EXAFS of calcined CuD16 (inset) and its FFT magnitude.

was to monitor CuO dispersion (via the lumping of the Cu−Cu second-shell EXAFS into a single Cu−Cu contribution) without relying on any potentially less stable, from a mathematical viewpoint, multi-shell fit. Figure 4 in the Supporting Information shows that, with the exception of small deviations at low k (possibly due to a small O contribution), the second shell is well represented by the parameters shown in Table 4.

The average Cu−Cu coordination number in the $Cu_6O_{16}^{20-}$ cluster shown in Figure 9, lower panel, is 3.3, which would be in agreement (within ±15% error) with our second-shell results. On the other hand, the Cu_{13} cluster shown in Figure 9 (O atoms have been omitted for clarity) is the "quasi-spherical" tenorite cluster that is closest in size to the preset dendrimer loading (16 Cu atoms). Its average Cu−Cu second-shell coordination number is 5.2. Since representation of the Cu−Cu second shell with a single Cu−Cu backscattering set was a compromise between accuracy and reliability of output parameters in multi-shell EXAFS fitting, we take the second-shell EXAFS analysis of calcined CuD16 as a semiquantitative indication of high CuO dispersion, since the Cu-computed second-shell coordination is severely depleted relative to that of the bulk.

Figure 11 summarizes our observations regarding the thermal evolution of our material. The Cu-loaded, trapped dendrimers are not geometrically arranged inside the sol−gel matrix (except for a possible constraint of a minimum dendrimer−dendrimer average distance) nor are the Cu^{2+} centers inside the dendrimer. We have arbitrarily assigned 15 Cu^{2+} centers to one dendrimer structure in Figure 11 and 17 centers to the other. In principle, one should expect the Cu^{2+}/dendrimer ratios in the trapped DAB-Am-64 species to be equal to 16, from a chemical equilibrium perspective, but strict adherence to it need not be exact. On calcination, very small CuO clusters trapped in a porous glass are formed.

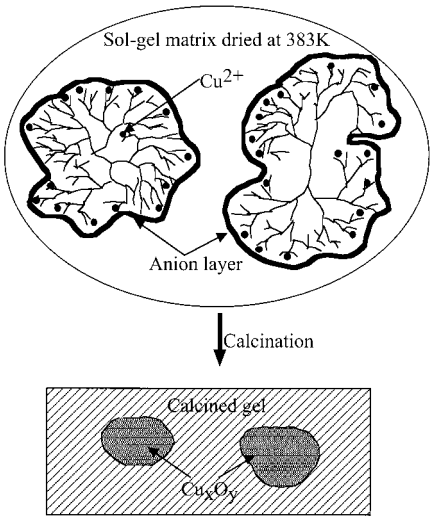

Figure 11. Qualitative description of calcined and uncalcined CuD16.

Acknowledgment. We acknowledge support from the NSF (CTS-9733756) and Kraft Foods Inc.

Supporting Information Available: EXAFS fitting figures for the calcined and uncalcined CuD16 Cu^{2+}/dendrimer/silica composite (PDF). This material is available free of charge via the Internet at http://pubs.acs.org.

CM010754S